2018

Dynamically integrated spatiotemporal-based trajectory planning and control for autonomous vehicles

Boyuan Li
University of Wollongong

Haiping Du
University of Wollongong, hdu@uow.edu.au

Weihua Li
University of Wollongong, weihuali@uow.edu.au

Bangji Zhang
Hunan University, bangjizhang@hnu.edu.cn

Dynamically integrated spatiotemporal-based trajectory planning and control for autonomous vehicles

Abstract

In the literature, the intensive research effort has been made on the trajectory planning for autonomous vehicles, while the integration of the trajectory planner with the trajectory controller is less focused. This study proposes the spatiotemporal-based trajectory planner and controller by a two-level dynamically integrated structure. In the upper level, the best trajectory is selected among a group of candidate time-parameterised trajectories, while the target vehicle ending position and velocity can be satisfied. Then the planned trajectory is evaluated by checking the feasibility when the actual vehicle dynamic motion constraints are considered. After that, the lower level trajectory controller based on the vehicle dynamics model will control the vehicle to follow the desired trajectory. Numerical simulations are used to validate the effectiveness of the proposed approach, where the scenario of an intersection and the scenario of overtaking are applied to show that the proposed trajectory controller can successfully achieve the control targets. In addition, compared with the potential field method, the proposed method based on the four-wheel independent steering and four-wheel independent driving electric vehicle shows great advantages in guaranteeing the vehicle handling and stability.

Disciplines

Engineering | Science and Technology Studies

Publication Details

B. Li, H. Du, W. Li & B. Zhang, "Dynamically integrated spatiotemporal-based trajectory planning and control for autonomous vehicles," IET Intelligent Transport Systems, vol. 12, (10) pp. 1271-1282, 2018.

Dynamically integrated spatiotemporal-based trajectory planning and control for autonomous vehicles

Boyuan Li [1,2], Haiping Du [2*], Weihua Li [3], Bangji Zhang[1]

[1] State Key Laboratory of Advanced Design and Manufacturing for Vehicle Body, Hunan University, Changsha 410082, China
[2] School of Electrical, Computer and Telecommunications Engineering, University of Wollongong, Wollongong, NSW 2522, Australia
[3] School of Mechanical, Material and Mechatronic Engineering, University of Wollongong, Wollongong, NSW 2522, Australia

[*]Corresponding author: hdu@uow.edu.au

Abstract: In the literature, intensive research effort has been made on the trajectory planning for autonomous vehicles, while the integration of the trajectory planner with trajectory controller is less focused. This study proposes the spatiotemporal-based trajectory planner and controller by a two-level dynamically integrated structure. In the upper level, the best trajectory is selected among a group of candidate time-parameterised trajectories, while the target vehicle ending position and velocity can be satisfied. Then the planned trajectory is evaluated by checking the feasibility when the actual vehicle dynamic motion constraints are considered. After that, the lower level trajectory controller based on vehicle dynamics model will control the vehicle to follow the desired trajectory. Numerical simulations are used to validate the effectiveness of the proposed approach, where the scenario of an intersection and the scenario of overtaking are applied to show that the proposed trajectory controller can successfully achieve the control targets. In addition, compared with the potential field method, the proposed method based on the four-wheel independent steering (4WIS) and four-wheel independent driving (4WID) electric vehicle shows great advantages in guaranteeing the vehicle handling and stability.

1. Introduction

In recent years, intensive research effort has been put on the area of autonomous driving due to the emerging technology of autonomous vehicles. Autonomous vehicles have the potential to improve the current transportation system, such as the accident prevention when the number of worldwide road accident is increasing [1][2]. In addition, the traffic and fuel efficiency can be improved by the autonomous traffic and fleet management system [3]. Within the realistic road traffic, however, the future autonomous vehicles will face the challenge of more dynamic and time-critical scenarios [4]. Thus, more complicated and reliable controllers are required to satisfy these challenges and requirements.

The development of autonomous vehicles can be classified as several stages according to [5]: in the earlier stage, various advanced driver assistance systems (ADAS), such as the lane departure warning (LDW), lane keeping assistance and cruise control system, were employed to assist the driving but driver was still in control of the vehicle; in the current stage, the entire trip is delegated to the autonomous control system so that the driver is not expected to perform any tasks, which can be considered as the fully autonomous control method.

Deep reinforcement learning has attracted the focused attention in the motion control of the fully autonomous vehicle in current literature. It is argued that the convolutional neural network (CNN) is an important approach to implement the deep learning and particularly suitable for imagine recognition [6]. CNN is widely applied to detect and classify pedestrians and vehicles, and is also utilised to implement the end-to-end framework of learning the autonomous control [6][7]. In [6], the image features were classified into different categories and influences of the image feature on the end-to-end learning performance of autonomous control by implementing CNN method were analysed. However, it was argued that the deep learning approach based on CNN could be only considered as the lowest recognition level of autonomous driving, and the more advanced deep learning methods for higher prediction level (based on recurrent neural network (RNN)) and planning level (based on reinforcement learning (RL) or deep Q networks (DQN)) were proposed in [8]. The major problem of the current deep reinforcement learning is the training procedure needs a large amount of labelled image data sets and the time integration of these image data also requires to predict, which is computational expensive and time-consuming. Wang et al. recently proposed an innovative deep learning framework for autonomous driving – parallel driving [9][10]. In parallel driving, the physical layer of vehicles and drivers and cybernetic layer of 'artificial drivers and artificial vehicles (ADAVs)' exist simultaneously. Based on cloud computing, the ADAVs are designed to implement the 'computational experiment' and deep reinforcement learning to carry out the trajectory planning and autonomous control of the artificial vehicles, and send the execute command to the physical vehicles. In this way, the computation burden of the local controller in individual physical vehicle is significantly reduced, but the computation load has transferred to the cybernetic layer and it is questionable whether the cybernetic layer can

successfully plan the detailed trajectories for thousands of vehicles simultaneously under the highly dynamic and complex street scenario. The major problem of the parallel driving and other deep learning method is the actual control performance and reliability is questionable under the complex scenarios. Furthermore, the trajectory planned by deep learning method does not consider the vehicle dynamics performance and the actual vehicle stability is questionable. Thus, the end-to-end autonomous control purely based on deep learning is questionable at current stage.

This study will focus on a more practical control framework for autonomous vehicle compared with deep learning method. Li et al. proposed a software system architecture for the trajectory planning and control of autonomous ground vehicle [11]. This system consisted of a number of modules, such as digital maps, perception and localisation system, behaviour planner, trajectory planner and trajectory controller. A manually constructed detailed digital map is applied, which provides various traffic information, such as lanes information and traffic information. In addition, the real-time vehicle position on the digital map can be determined by the perception and localisation system (the GPS combined with IMU and wheel encoder). Based on the digital map and vehicle's real-time position on the digital map, the behavioural planner is responsible for making deliberate manoeuvre task decisions, such as lane following, lane changing, vehicle following and overtaking, in complex street-driving scenario. The global route planner in the behaviour level can compute the rough reference path while stratifying the task decisions. Then in the trajectory planning and trajectory tracking level, the planned and tracked trajectory should follow the rough reference path.

In this study, the rough reference path is assumed to be known and the trajectory planning and tracking control level controller is mainly focused. According to vehicle sensors and surrounding environment, the high-level trajectory planner considers both the information of the guidance path and vehicle motion constraints and selects the best vehicle trajectory. Then the low-level trajectory controller will control the individual vehicle actuator to achieve the selected trajectory. The high-level motion planning control method can be classified as the spatial-based method and the spatiotemporal-based method. The spatial-based method is widely used in the literature to plan the trajectory only in the spatial dimension and this method does not explicitly account for the time parameter [12]. Specifically, in the direct tracking method, the desired path is determined at first and the steering system is controlled to follow the desired path exactly at every time step [13][14]. In the potential field method, the steering control method based on the potential fields can form a steering corridor with a desired tracking error tolerance and the vehicle can be steered smoothly with smaller control effort compared with the direct tracking method [15]. However, during rushing nose-to-tail traffic, the spatial-based approaches quickly reach their limits and lead to poor performance or even accidents [16]. This leads to the development of the spatiotemporal-based trajectory planning concept, where time parameterised trajectories are created by considering the kinematic constraints. Typical spatiotemporal-based planning methods have been proposed to find the trajectory connecting the initial state with an exactly defined goal state [17][18][19]. These methods relied on discrete geometric structure, such as the rapidly exploring random trees (RRT) [20] and state lattice [19]. However, when the surrounding environment is unconstructed and complex, these methods may not quickly generate the alternative trajectory. The trajectory planning strategies proposed in [21][22] take the advantage of 'deliberated multiple final states', which have multiple alternative final states and are highly responded to traffic changes. In study [4], the combined optimization of the longitudinal and lateral moment are proposed and the multiple target positions are described as the offset error values from the target reference positions. In addition, in order to create time parameterised trajectory and account for the kinematic constraints, the terminal time can be selected and the derivative of desired target positions should satisfy certain reference values.

It is also vital for the optimal trajectory-based planning to achieve the safe and human-comfort vehicle motion. In [23], it is suggested that nature paths are those that resemble human generated paths. Executing familiar manoeuvres would surely contribute to the passenger comfort improvement. Thus, the studies [4][24] propose the trajectory-based planning method and this method can achieve the human-like trajectory generation and fast determine the global trajectory. The optimal targets of this proposed optimal trajectory generation method are the minimising of the square of the longitudinal and lateral jerk, the minimising of the total time and the minimising of the trajectory tracking error.

Most of the studies in the literature, however, only focused on the vehicle trajectory planning but less of the studies dynamically integrated the actual vehicle dynamics performance and trajectory control together. In [25], an integrated local trajectory planning and tracking control framework were proposed and dynamics-model based predictive path generation algorithm was applied to plan a set of smooth and kinematically-feasible path. It is suggested in [26] that bicycle or car-like kinematic model are widely used to exploit the basic manoeuvre capability of the car, but the comprehensive vehicle dynamics model which considers the tyre-road friction coefficient and limits of the specific tyre force has been applied in few studies.

In this study, a two-level real-time dynamically integrated spatiotemporal-based trajectory planning and control method is proposed. The upper level vehicle trajectory planner can successfully generate the spatiotemporal-based trajectories with various terminal time and state ending conditions. Among these trajectories, the best suitable trajectory is selected based on the optimised cost function which is used to minimise the tracking error and terminal time spent. In the proposed trajectory planner, the curvature discontinuities at the conjunction of the line segments and arcs can be prevented by the generated human-like path. After that, according to the required vehicle velocity and yaw rate from the generated trajectory, the comprehensive vehicle dynamics model is applied to check whether this actual trajectory can be implemented. This feasibility check includes the checking of the feasibility of the required longitudinal acceleration and whether the tyre remains in the linear stability region for the actual vehicle. After the feasibility analysis of the planned trajectory, this study includes the trajectory controller in the

lower level based on the sliding-mode method and vehicle dynamics model to validate that the vehicle can be controlled successfully according to the selected best suitable trajectory. The 4WIS-4WID electric vehicle shows advantages over the traditional vehicle due to the availability of more control actuators, and therefore the advantage of implementing 4WIS-4WID model on autonomous control compared with traditional two-wheel model is also discussed.

The structure of this paper is organised as follows: first, the 4WIS-4WID vehicle dynamics model and traditional two-wheel dynamics model for autonomous vehicles are described. Then the proposed trajectory planner in the upper level is described and the feasibility analysis of the planned trajectory is implemented. After that, the vehicle trajectory controller based on the vehicle dynamics model is presented. Finally, simulations are carried out to compare the different controllers and verify the effectiveness of the proposed controllers.

2. Vehicle dynamics model

In this paper, a 4WIS-4WID vehicle model is utilised first to describe the dynamic motion of an autonomous vehicle. This model simulates the conditions of a real vehicle, and is used to validate the performance of the proposed trajectory control method.

The equations of motion of this model are described as follows:

$$m\dot{v}_x = mv_y r + \left(F_{xfl} + F_{xfr} + F_{xrl} + F_{xrr}\right) \tag{1a}$$

$$m\dot{v}_y = -mv_x r + \left(F_{yfl} + F_{yfr} + F_{yrl} + F_{yrr}\right) \tag{1b}$$

$$I_z\dot{r} = l_f\left(F_{yfl} + F_{yfr}\right) - l_r\left(F_{yrl} + F_{yrr}\right) + \frac{b_f}{2}\left(F_{xfl} - F_{xfr}\right) + \frac{b_r}{2}\left(F_{xrl} - F_{xrr}\right) \tag{1c}$$

where v_x, v_y, r are the vehicle longitudinal velocity, lateral velocity, and yaw rate, respectively. $F_{xfl}, F_{xfr}, F_{xrl}, F_{xrr}$ are the vehicle front left, front right, rear left and rear right longitudinal tyre forces, respectively, and $F_{yfl}, F_{yfr}, F_{yrl}, F_{yrr}$ are the vehicle front left, front right, rear left and rear right lateral tyre forces, respectively. l_f and l_r are the front and rear wheel base lengths, while b_f and b_r are the front and rear track widths. I_z and m are the moment of vehicle inertia in terms of yaw axis and vehicle mass.

The tyre traction or brake force and side force are defined as F_{ti} and F_{si}, respectively, which can be related to the longitudinal and the lateral tyre forces by the steering angle δ_i as follows:

$$\begin{aligned} F_{xi} &= F_{ti}\cos\delta_i - F_{si}\sin\delta_i \\ F_{yi} &= F_{ti}\sin\delta_i + F_{si}\cos\delta_i \end{aligned} \tag{2}$$

where $i = fl, fr, rl, rr$, which represents the front left, front right, rear left and rear right wheel, respectively.

The non-linear Dugoff tyre model is used in this paper [27], and is described by:

$$\begin{aligned} \lambda_i &= \frac{\mu F_{zi}\left[1 - \varepsilon_r u_i\sqrt{s_i^2 + \tan^2\alpha_i}\right](1 - s_i)}{2\sqrt{C_s^2 s_i^2 + C_\alpha^2\tan^2\alpha_i}} \\ f(\lambda_i) &= \begin{cases} \lambda_i(2 - \lambda_i) & (\lambda_i < 1) \\ 1 & (\lambda_i > 1) \end{cases} \\ F_{si} &= \frac{C_\alpha\tan\alpha_i}{1 - s_i} f(\lambda_i) \\ F_{ti} &= \frac{C_s s_i}{1 - s_i} f(\lambda_i) \end{aligned} \tag{3}$$

where μ is the tyre-road friction coefficient. F_{zi} is the vertical load of each wheel. C_s is the longitudinal cornering stiffness and C_α is the lateral cornering stiffness. s_i is the longitudinal slip ratio, and α_i is the lateral slip angle. ε_r is a constant value, and u_i is the vehicle velocity component in the wheel plane.

The wheel rotation dynamics is described by the following equation:

$$I_\omega\dot{\omega}_i = -R_\omega F_{ti} + T_i \tag{4}$$

For the traditional two-front-wheel steering vehicle, the dynamics equation can be simplified as:

$$m\dot{v}_x = mv_y r + F_{tfl} + F_{tfr} - F_{sfl}\sin\delta - F_{sfr}\sin\delta \tag{5a}$$

$$m\dot{v}_y = -mv_x r + F_{sfl}\cos\delta + F_{sfr}\cos\delta + F_{srl} + F_{srr} \tag{5b}$$

$$I_z\dot{r} = l_f\left(F_{sfl}\cos\delta + F_{sfr}\cos\delta\right) - l_r\left(F_{srl} + F_{srr}\right) + \frac{b_f}{2}\left(-F_{sfl}\sin\delta + F_{sfr}\sin\delta\right) \tag{5c}$$

where δ is the front wheel steering angle.

3. Trajectory planner

The whole structure of the proposed dynamically integrated trajectory planning and control method mainly includes the upper level trajectory planner, the lower level trajectory controller, and the vehicle dynamics model, which is presented in Figure 1.

It is assumed the desired vehicle initial and ending states of each section of the road along the rough reference path have already known in advance. These reference values are determined by the behaviour layer task planner and digital map. This is a reasonable assumption because many studies in the literature have determined the rough reference path by behaviour level task planner based on digital map [11][28][29].

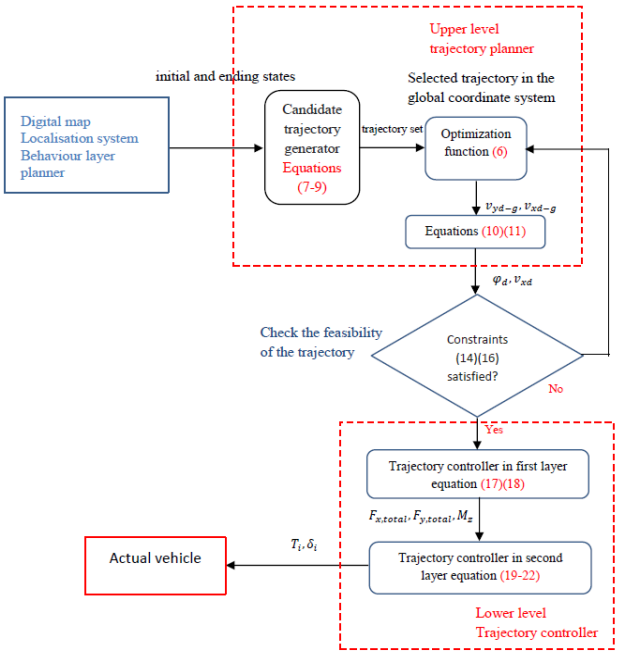

Figure 1. *The whole control structure of the dynamically integrated trajectory planning and control method.*

3.1 Trajectory planner

In the proposed trajectory planner, the multiple target positions in each road section are defined as a group of offset longitudinal positions and a group of offset lateral positions from the reference values. The start state of is assumed as $[d_0 \quad \dot{d}_0 \quad \ddot{d}_0]$ and the desired ending state is assumed as $[d_1 \quad \dot{d}_1 \quad \ddot{d}_1]$. d_1 is a group of offset positions which is constrained within the road boundary and d_0 is the initial condition. $\dot{d}_0$ and $\ddot{d}_0$ present the initial velocity and acceleration, while $\dot{d}_1$ and $\ddot{d}_1$ present the ending velocity and acceleration. In order to guarantee the continuities of the planned trajectory, the initial state d_0 in this section of road should be the ending state of previous section. Since the selection of terminal time and the selection of offset error from desired final states can both affect the trajectory planning and tracking control performance, the terminal cost function $h(d_1, \tau) = k_\tau \tau + k_{d_1}\left(d_r - d_1(\tau)\right)^2$ is designed to balance the terminal time cost and offset error from desired state. d_r is the reference vehicle state. k_j and k_d are the scaling factors of each term. The vehicle trajectory tracking behaviour is strongly affected by the selection of terminal time: the small terminal time can reach the final states early, which leads to uncomfortable, energetically wasteful actions, while large terminal time with late arrival on final states implies slow but stable movements. If we want to minimise the terminal time, the gain value k_τ is selected as the value much bigger than k_{d_1}. If we want to minimise the offset error from the reference value, then vice versa.

Furthermore, the vehicle longitudinal or lateral jerk $\dddot{d}(\tau)$ should be minimised to improve the smoothness of the trajectory. The total cost function J can be presented as:

$$\sum_{d_1,\tau} J_1 = k_j \left(\dddot{d}_1(\tau)\right)^2 + h(d_1, \tau) \tag{6}$$

where k_j scaling factor of the term related to longitudinal or lateral jerk. τ is the candidate terminal time of this section of the road and $\tau \in [0 \quad T]$. T is the longest time required to complete the motion. In each section of the road, a whole trajectory set is generated by combing different end conditions d_{1i} and τ_j [4], where i, j mean that the trajectory planner will generate the number of $i \times j$ trajectories. d_{1i} is the ith number of the target final position of this section of road and would close to the target position when $d_{1i} \to d_1$. τ_j is the jth number of terminal time of this section of road. The optimisation algorithm will choose the best trajectory based on the cost function (6) from these $i \times j$ trajectories. It can be also noted that the target final velocity $\dot{d}_{1i}$ or acceleration $\ddot{d}_{1i}$ can be used in (6) instead of d_{1i} if the final velocity or acceleration is required to be optimised.

Assume the vehicle trajectory $d(\tau)$ in the optimisation problem can be described by the following quintic state equations [4]:

$$d_1 = c_0 + c_1 t + c_2 t^2 + c_3 t^3 + c_4 t^4 + c_5 t^5 \tag{7a}$$
$$\dot{d}_1 = c_1 + 2c_2 t + 3c_3 t^2 + 4c_4 t^3 + 5c_5 t^4 \tag{7b}$$
$$\ddot{d}_1 = 2c_2 + 6c_3 t + 12c_4 t^2 + 20c_5 t^3 \tag{7c}$$

with $c_0, c_1, \dots, c_5 \in R$ and $t \in [0 \quad \tau]$.

Equation (7) can be rewritten as the following equation:

$$\boldsymbol{\xi}(t) = \boldsymbol{M_1}(t)\boldsymbol{c_{012}} + \boldsymbol{M_2}(t)\boldsymbol{c_{345}} \tag{8}$$

where $\boldsymbol{M_1}(t) = \begin{bmatrix} 1 & t & t^2 \\ 0 & 1 & 2t \\ 0 & 0 & 2 \end{bmatrix}$, $\boldsymbol{M_2}(t) = \begin{bmatrix} t^3 & t^4 & t^5 \\ 3t^2 & 4t^3 & 5t^4 \\ 6t & 12t^2 & 20t^3 \end{bmatrix}$, $\boldsymbol{\xi}(t) = \begin{bmatrix} d(t) \\ \dot{d}(t) \\ \ddot{d}(t) \end{bmatrix}$.

According to the initial and final states, the coefficients $[c_0, c_1, c_2, c_3, c_4, c_5]$ of the quintic state trajectory can be calculated:

$$\boldsymbol{c_{012}} = \begin{bmatrix} c_0 \\ c_1 \\ c_2 \end{bmatrix} = \boldsymbol{M_1}(0)^{-1}\boldsymbol{\xi_0} \tag{9a}$$

$$\boldsymbol{c_{345}} = \begin{bmatrix} c_3 \\ c_4 \\ c_5 \end{bmatrix} = \boldsymbol{M_2}(\tau)^{-1}[\boldsymbol{\xi_t} - \boldsymbol{M_1}(\tau)\boldsymbol{c_{012}}] \tag{9b}$$

where $\boldsymbol{M_1}(0) = \begin{bmatrix} 1 & 0 & 0 \\ 0 & 1 & 0 \\ 0 & 0 & 2 \end{bmatrix}$, $\boldsymbol{\xi_0} = \begin{bmatrix} d_0 \\ \dot{d}_0 \\ \ddot{d}_0 \end{bmatrix}$ and $\boldsymbol{\xi_t} = \begin{bmatrix} d_1 \\ \dot{d}_1 \\ \ddot{d}_1 \end{bmatrix}$.

After the above coefficients are calculated, the vehicle trajectory can be described as $d_1(t)$ in equation (7a). In this way, these $i \times j$ trajectories in this section of the road can be calculated and the best trajectory can be selected based on the optimisation of the cost function.

The above optimisation cost function (6) is only corresponding to one section of road. If the rough desired path is divided into several sections of road by a set of position points, a number of the optimisation calculations are implemented successively. In the ideal condition, the more sections the pre-defined path is divided, the more accurate the optimisation results would be. However, this requires intensive computing efforts and the balance between the optimisation performance and the calculation effects should be achieved.

Vehicle trajectory planning in the global coordinate system in this study can be divided as the longitudinal trajectory planning and the lateral trajectory planning. Equations (6-9) provide the common optimisation algorithm for both the longitudinal trajectory and lateral trajectory.

After the desired trajectory is proposed with certain position constraints and velocity constraints, the next stage is to map the desired trajectory into the desired longitudinal velocity and yaw angle in the vehicle body-fixed coordinate system. According to the longitudinal velocity and lateral velocity of the desired trajectory in the global coordinate system, the desired yaw angle φ_d and longitudinal velocity v_{xd} in the body-fixed coordinate system can be optimised according to the following equation:

$$J_{2min,\varphi_d,v_{xd}} = a\left(v_{xd}(k) - v_{xd-b}(k)\right)^2 + b\left(v_{xd}\tan\varphi_d(k) - v_{yd-b}(k)\right)^2 + c\left(\varphi_d(k) - \varphi_d(k-1)\right)^2 \quad (10)$$

where a, b and c are scaling factors, which are used to achieve the desired longitudinal velocity, lateral velocity and avoid the abrupt change of the yaw angle between each time step and improve the smooth of the trajectory. k presents the time step $t(k)$ and $k-1$ presents the time step $t(k-1)$. v_{xd-b} and v_{yd-b} represent the desired longitudinal velocity and lateral velocity in the body-fixed coordinate system, which can be calculated according to the desired longitudinal velocity v_{xd-g} and lateral velocity v_{yd-g} in the global coordinate system:

$$v_{xd-b} = v_{xd-g}\cos\varphi + v_{yd-g}\sin\varphi \quad (11a)$$

$$v_{yd-b} = v_{xd-g}\sin\varphi - v_{yd-g}\cos\varphi \quad (11b)$$

When v_{xd} and φ_d are determined, the trajectory planning has finished and the desired tyre forces and yaw moment can be calculated by the trajectory controller.

It is noted that the optimization target of the last term in the optimization problem (10) is less important than the primary optimization target of achieving the planned longitudinal and lateral velocities, so the scaling factor c can be set much smaller than a, b.

3.2 Dynamically checking the feasibility of the planned trajectory

In order to successfully complete the planned motion, the actual autonomous vehicle should be able to achieve desired longitudinal acceleration $\dot{v}_{xd}$ and yaw rate $\dot{\varphi}_d$ in the vehicle body-fixed coordinate system.

For the traditional vehicle, based on the centralised powertrain distribution pattern, the maximum longitudinal acceleration a_{xm} can be generated is:

$$a_{xm} = \pm\frac{T_M}{R_\omega m} - C_r g - \frac{D_a v_x^2}{m} \quad (12)$$

where T_M is the electric vehicle's total maximum available driving/braking torque. C_r is the rolling resistance coefficient and D_a is the wind drag coefficient.

For the 4WIS-4WID electric vehicle, based on the decentralised powertrain distribution pattern, the maximum longitudinal acceleration which can be generated is:

$$a_{xm} = \pm\frac{4T_m}{R_\omega m} - C_r g - \frac{D_a v_x^2}{m} \quad (13)$$

where T_m is the electric vehicle's maximum available driving/braking torque of individual wheel.

If the following condition is satisfied, the planned trajectory is feasible for the longitudinal acceleration:

$$\dot{v}_{xd} < |a_{xm}| \quad \text{when vehicle is accelerating} \quad (14a)$$

$$\dot{v}_{xd} > -|a_{xm}| \quad \text{when vehicle is braking} \quad (14b)$$

In addition, the stability analysis of the vehicle system is also required in the trajectory feasibility analysis. In Dugoff tyre model, the stability region is defined as the linear region and nonlinear region according to equation (3).

In equation (3), λ_i presents the linearity of each tyre. In order to guarantee the feasibility of the trajectory, λ_i should be larger than 1 and the tire is working in the linear tyre region. According to equation (3), a number of vehicle states affect λ_i, such as the vehicle side-slip angle, slip ratio, vertical load and tyre-road friction coefficient. Thus, in the trajectory feasibility analysis, it is hard to determine the exact λ_i mathematically.

Table 1 shows the maximum yaw rate within the linear stability region which are obtained from the simulation results using the vehicle dynamics model (1)-(4) and parameters given in Table 2 under different initial conditions with sinusoidal steering input. In the simulation, the λ_i value of an individual wheel has been plotted and checked. If the λ_i value of a specific tyre is less than 1 (larger than 1), this specific tyre is working in the nonlinear tyre region (linear tyre region). The maximum yaw rate within the linear stability region can be defined as the maximum yaw rate value when all the λ_i values of four tyres are larger than 1. It is noted that rather than used to show the maximum yaw rate constraints, the defined maximum yaw rate in this paper is used to prevent the vehicle tyre from working in the undesired nonlinear tyre region. Table 1 also shows that the 4WIS-4WID vehicle has larger yaw rate threshold value in the linear tyre region than the traditional two-wheel vehicle. It is also noted that Table 1 only shows the maximum yaw rate of the fixed initial longitudinal velocity. However, the longitudinal velocity v_x would change continuously in the real situation. In order to obtain the real-time value of maximum yaw rate to check the feasibility, the interpolation method is applied:

$$r_{max} = \frac{v_{02} - v_x}{v_{02} - v_{01}} r_{max1} + \frac{v_x - v_{01}}{v_{02} - v_{01}} r_{max2} \quad (15)$$

It is assumed that the real-time velocity is between the fixed velocities v_{01} and v_{02} in Table 1. r_{max1} and r_{max2} are the corresponding maximum yaw rate of v_{01} and v_{02}.

Remark: The maximum yaw rate in Table I is obtained by the simulations with sinusoidal steering input and certain initial longitudinal velocity. Since the longitudinal velocity will remain almost unchanged by velocity controller, the obtained maximum yaw rate r_m can be simply considered as the maximum yaw rate under the initial longitudinal velocity v_0.

In order to guarantee the stability, the desired yaw rate of the planned trajectory should satisfy the following equation:

$$\dot{\varphi}_d < |r_m| \quad \text{when } \dot{\varphi}_d > 0 \quad (16a)$$

$$\dot{\varphi}_d > -|r_m| \quad \text{when } \dot{\varphi}_d < 0 \quad (16b)$$

where r_m is the maximum value of the yaw rate in the linear stability region.

Table 1. The maximum yaw rate within the linear stability region (rad/sec)

	$\mu = 0.9$		$\mu = 0.5$	
	Two-wheel vehicle	4WIS-4WID vehicle	Two-wheel vehicle	4WIS-4WID vehicle
v_0=20 m/s	±0.222	±0.222	±0.124	±0.124
v_0=15 m/s	±0.289	±0.289	±0.156	±0.157
v_0=10 m/s	±0.415	±0.440	±0.225	±0.244
v_0=5 m/s	±0.488	±0.555	±0.312	±0.367

If both of conditions (14) and (16) are satisfied, the planned trajectory is feasible and the trajectory controller can be applied accordingly. If these conditions are unsatisfied, the cost function (6) can be revised as follows:

$$\sum_{d_1,\tau} J_1 = k_j \left(\ddot{d}_1(\tau)\right)^2 + h(d_1,\tau) + K_{un} \tag{6}$$

where K_{un} is extremely large positive value, which is utilised to increase the total cost of the selected ending position and terminal time and consequently the alternative route can be selected.

4. Vehicle trajectory controller

In this section, the vehicle two-layer trajectory controller is proposed to control the autonomous vehicle to follow the desired planned trajectory. In the first layer, the desired longitudinal force, lateral force and yaw moment in the vehicle body-fixed coordinate system can be calculated according to the desired longitudinal velocity, lateral velocity and yaw angle. In addition, the actual values of longitudinal velocity, lateral velocity and yaw angle are also required in the first layer as the actual feedback values in the trajectory controller. The second layer is the execute layer, which can control and optimise the individual steering and driving actuators to achieve the desired longitudinal force, lateral force and yaw moment.

4.1 Trajectory controller in the first layer

The vehicle tracking error dynamics equation can be presented by the following equation based on [30]:

$$\tilde{v}_y = \left[v_x \sin\tilde{\varphi} + v_y \cos\tilde{\varphi}\right] - v_{yd} \tag{17a}$$

$$\tilde{v}_x = \left[v_x \cos\tilde{\varphi} - v_y \sin\tilde{\varphi}\right] - v_{xd} \tag{17b}$$

$$\tilde{\varphi} = \varphi_{act} - \varphi_d \tag{17c}$$

where φ_{act} is the actual vehicle yaw angle. $\tilde{v}_x$ and $\tilde{v}_y$ are longitudinal velocity error and lateral velocity error, respectively. In order to improve the vehicle stability and minimise the vehicle body side-slip angle, the desired lateral velocity v_{yd} is assumed as zero value.

The vehicle trajectory controller adds up both the feedforward and feedback force and moment demands:

$$F_{x,total} = m\dot{v}_{xd} - m\tilde{v}_y\dot{\varphi}_d - K_1\tilde{v}_x \tag{18a}$$

$$F_{y,total} = mv_{xd}\dot{\varphi}_d + m\tilde{v}_x\dot{\varphi}_d - K_{2p}\tilde{v}_y - K_{2d}\dot{\tilde{v}}_y \tag{18b}$$

$$M_z = I_z\ddot{\varphi}_d - K_{3p}\tilde{\varphi} - K_{3d}\dot{\tilde{\varphi}} \tag{18c}$$

where $K_1, K_{2p}, K_{2d}, K_{3p}, K_{3d}$ are feedback control gains. $F_{x,total}$ and $F_{y,total}$ are the total desired longitudinal tyre force and total lateral tyre force, respectively.

4.2 Trajectory controller in the second layer

In this study, vehicle dynamics model is also used in the second layer controller to generate controlled steering angle and driving/braking torque and achieve trajectory control targets. In this section, the 4WIS-4WID vehicle model is used as an example to achieve the desired trajectory control.

In this section, the control targets of the actuator control allocation method are the desired total longitudinal tyre force, the desired total lateral tyre force and desired yaw moment determined in the first layer trajectory controller in the last section. In addition, the individually allocated tyre forces are minimised to guarantee each tyre has been used sufficiently. The cost function of this actuator control allocation problem is shown as follows:

$$J_{3min,F_{ti},F_{si}} = \frac{F_{tfl}^2 + F_{sfl}^2}{\mu^2 F_{zfl}^2} + \frac{F_{tfr}^2 + F_{sfr}^2}{\mu^2 F_{zfr}^2} + \frac{F_{trl}^2 + F_{srl}^2}{\mu^2 F_{zrl}^2} + \frac{F_{trr}^2 + F_{srr}^2}{\mu^2 F_{zrr}^2} \tag{19}$$

subject to:

$$\boldsymbol{B_x F} = F_{x,total} \tag{19a}$$

$$\boldsymbol{B_y F} = F_{y,total} \tag{19b}$$

$$\boldsymbol{B_r F} = M_{z,total} \tag{19c}$$

where $\boldsymbol{F} = \begin{bmatrix} F_{tfl} \\ F_{tfr} \\ F_{trl} \\ F_{trr} \\ F_{sfl} \\ F_{sfr} \\ F_{srl} \\ F_{srr} \end{bmatrix}$,

$$\boldsymbol{B_x} = [\cos\delta_{fl} \quad \cos\delta_{fr} \quad \cos\delta_{rl} \quad \cos\delta_{rr} \quad -\sin\delta_{fl} \quad -\sin\delta_{fr} \quad -\sin\delta_{rl} \quad -\sin\delta_{rr}]$$

$$\boldsymbol{B_y} = [\sin\delta_{fl} \quad \sin\delta_{fr} \quad \sin\delta_{rl} \quad \sin\delta_{rr} \quad \cos\delta_{fl} \quad \cos\delta_{fr} \quad \cos\delta_{rl} \quad \cos\delta_{rr}]$$

$$\boldsymbol{B_r} = [l_f\sin\delta_{fl} + 0.5b_f\cos\delta_{fl} \quad l_f\sin\delta_{fr} - 0.5b_f\cos\delta_{fr} \quad -l_r\sin\delta_{rl} + 0.5b_r\cos\delta_{rl} \quad -l_r\sin\delta_{rr} - 0.5b_r\cos\delta_{rr} \quad l_f\cos\delta_{fl} - 0.5b_f\sin\delta_{fl} \quad l_f\cos\delta_{fr} + 0.5b_r\sin\delta_{fr} \quad -l_r\cos\delta_{rl} - 0.5b_r\sin\delta_{rl} \quad -l_r\cos\delta_{rr} + 0.5b_r\sin\delta_{rr}]$$

$$F_{ti}^2 + F_{si}^2 \le \mu F_{zi}^2 \tag{19d}$$

where F_x, F_y are the actual total longitudinal tyre force and lateral tyre force. $M_z = I_z\dot{r}$ is the actual yaw moment of the vehicle. F_{zi} is the vertical load of each individual wheel. These values are all hard to measure and can be determined by the 4WIS-4WID vehicle dynamics model when given the input values (steering angle and traction/brake torque) to the dynamics model.

The constraints (19a), (19b) and (19c) are applied here to achieve the desired longitudinal tyre force, lateral tyre force and yaw moment. To overcome the distribution error due to the non-linear characteristic of the vehicle dynamics model, the sliding mode controller (SMC) is proposed in constraints (19a), (19b) and (19c) to accurately tracking the desired values.

The SMC control law can be chosen as following equations to replace the constraints (19a)-(19c):

$$\boldsymbol{B_x F} = F_{x,total} - K_{s1}\,\mathrm{sgn}\,S_1 \quad (20a)$$

$$\boldsymbol{B_y F} = F_{y,total} - K_{s2}\,\mathrm{sgn}\,S_2 \quad (20b)$$

$$\boldsymbol{B_r F} = M_{z,total} - K_{s3}\,\mathrm{sgn}\,S_3 \quad (20c)$$

where K_{s1}, K_{s2} and K_{s3} are control gains of SMC, which are all positive values. In order to achieve good control performance, these control gains can be set as large values, but too large control gains may lead to the large oscillation of the control output values. The sliding surface S_1, S_2 and S_3 can be presented as followings:

$$S_1 = \int \boldsymbol{B_x F} - F_{x,total} \quad (21a)$$

$$S_2 = \int \boldsymbol{B_y F} - F_{y,total} \quad (21b)$$

$$S_3 = \int \boldsymbol{B_r F} - M_{z,total} \quad (21c)$$

The stability of suggested SMC can be proved by the Lyapunov method, which is shown in the Appendix.

The effect of tyre friction circle is considered in (19d). The optimisation problem (19) can be solved by the Matlab embedded function 'fmincon' and the detailed analysis of the optimisation algorithm is beyond the scope of this study.

When the individual tyre forces have been allocated in (20), the controlled value of individual actuator can be mapped from the individual tyre force by the following equations:

$$T_i = F_{ti} R_\omega \quad (22a)$$

$$\delta_{fl} = \frac{F_{sfl}}{C_\alpha} + \frac{l_f r}{v_x} \quad (22b)$$

$$\delta_{fr} = \frac{F_{sfr}}{C_\alpha} + \frac{l_f r}{v_x} \quad (22c)$$

$$\delta_{rl} = \frac{F_{srl}}{C_\alpha} - \frac{l_r r}{v_x} \quad (22d)$$

$$\delta_{rr} = \frac{F_{srr}}{C_\alpha} - \frac{l_r r}{v_x} \quad (22e)$$

This controlled actuator values can be sent as the control signal to actual electric vehicle to achieve desired vehicle motion.

5. Simulation results

In this section, three sets of simulation results are used to verify the effectiveness of proposed trajectory planner and controller. In the first set of simulations, the simulation scenario of the intersection is presented and the controlled vehicle intends to go through the intersection and make the right turn. In the second and third set of simulations, the controlled vehicle is overtaking the vehicle ahead in the same lane. For the purpose of comparison, the control performance of the potential field method based on [9] is presented here to show the advantage of proposed method. The simulation parameters are shown in Table 2.

Table 2. Parameter values used in simulations [31].

m	Mass	1298.9 kg
l_f	Distance of c.g. from the front axle	1 m
l_r	Distance of c.g. from the rear axle	1.454 m
b_f	Front track width	1.436 m
b_r	Rear track width	1.436 m
C_s	Longitudinal stiffness of the tyre	50000 N/unit slip ratio
I_z	Vehicle moment of inertial about yaw axle	1627 kgm^2
R_ω	Wheel radius	0.35 m
I_ω	Wheel moment of inertial	2.1 kgm^2
ε_r	Road adhesion reduction factor	0.015 s/m
C_α	Cornering stiffness of the tyre	30000 N/rad
T_m	Maximum driving or brake torque	500 N.m (-500 N.m)

In the first set of simulation, it is assumed that the controlled vehicle is moving along the left lane of the road and then this vehicle is planning to have the right turn in the intersection. The desired initial velocity of the vehicle is 20 m/s and the velocity decreases steadily into 2 m/s at point A. After that, the vehicle starts to make the right turn with relative low speed. The longitudinal velocity should increase from 2 at point A into 3 m/s at point B and the lateral velocity should increase from 0 at point A into 2 m/s at point B. This scenario is depicted in Figure 2(a). The tyre-road friction coefficient is 0.9 in all the simulations in this section.

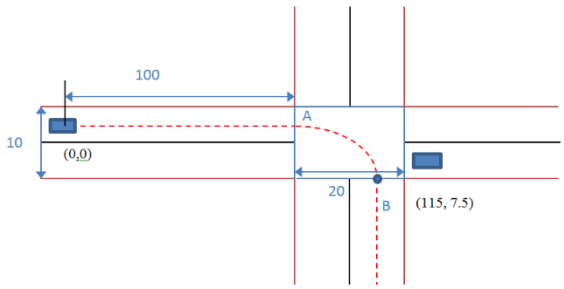

(a)

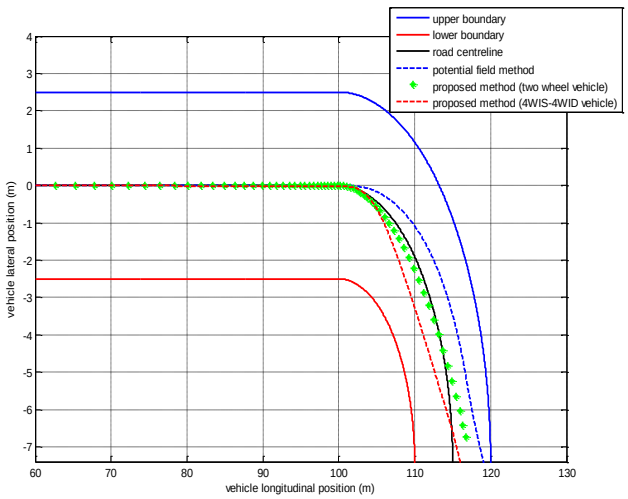

(b)

***Figure 2**. **(a)** The first scenario in the intersection (unit: meter) **(b)** The vehicle trajectory in the global coordinate system.*

The road centreline and road boundary can be shown in Figure 2(b). The planned trajectory in the proposed method includes two stages: vehicle straight motion in the left lane and vehicle turning motion in the intersection. The

actual vehicle trajectory for the 4WIS-4WID vehicle and two-wheel vehicle and the planned desired trajectory are plotted together in Figure 2(b). In addition, for the purpose of comparison, the 4WIS-4WID vehicle trajectory controlled by the potential filed method [9] is also shown. According to Figure 2(b), all the proposed method and the potential field method can guarantee the controlled vehicle is moving within the road boundary.

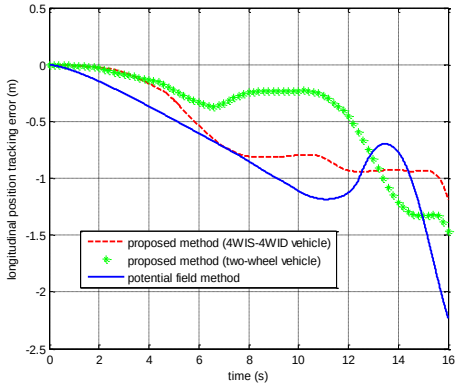

(a)

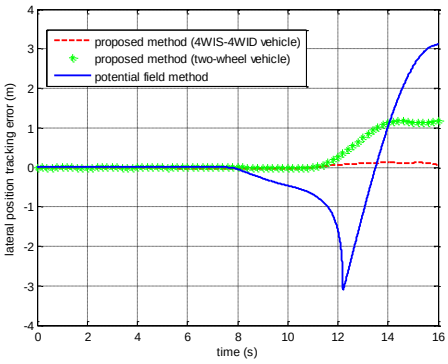

(b)

***Figure 3**. The tracking errors of vehicle trajectory in the first set of simulations **(a)** longitudinal position **(b)** lateral position.*

Figure 3(a) and 3(b) plot the tracking error of all the methods in the longitudinal direction and lateral direction. The proposed methods based on two-wheel model and 4WIS-4WID model both show better tracking performance compared with the potential field method on longitudinal direction and lateral direction. Since 4WIS-4WID vehicle has better mobility, the proposed method applied on 4WIS-4WID has much smaller tracking error of lateral position compared with two-wheel model.

Figure 4(a) and 4(b) present the longitudinal velocity and lateral velocity in the global coordinate system for both the potential field method and the proposed trajectory planning method. It is noted that in order to achieve better optimization performance, the proposed trajectory tracking controller is not required to follow the strictly-defined reference velocity, but only need to satisfy the desired velocities on initial and ending reference points. The target longitudinal velocities on point A and point B are shown as V_{xd1} and V_{xd2} in Figure 4(a), while the target lateral velocities on point A and point B are shown as V_{yd1} and V_{yd2} in Figure 4(b). The proposed method can achieve the target longitudinal velocity and lateral velocity at point A and point B, while the potential field method cannot achieve the target velocities especially the lateral velocity. This is because that only the vehicle longitudinal velocity can be controlled and the vehicle motion is constrained within a specific boundary for the potential field method, while the proposed method can optimise both the spatiotemporal-based longitudinal and lateral trajectory and satisfy certain target ending velocity constraints. This is the major difference between the spatial-based path-based method (potential field method) and the proposed spatiotemporal-based trajectory planning method.

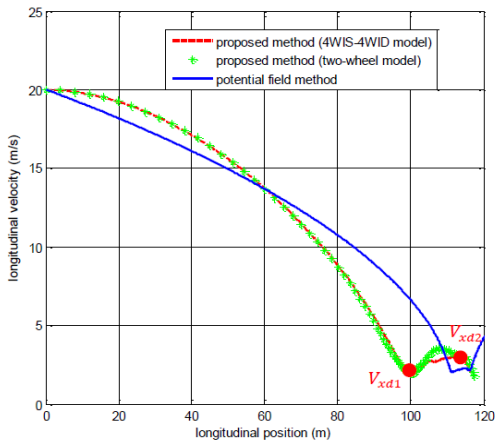

(a)

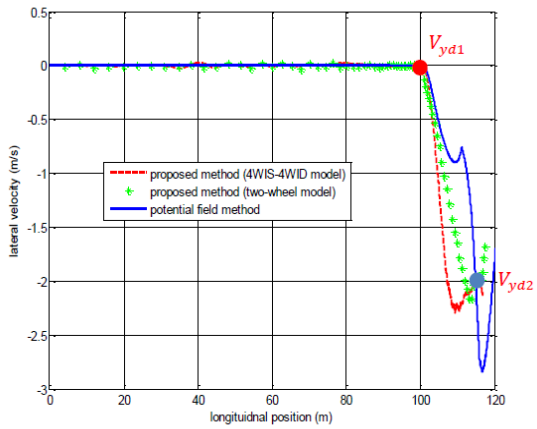

(b)

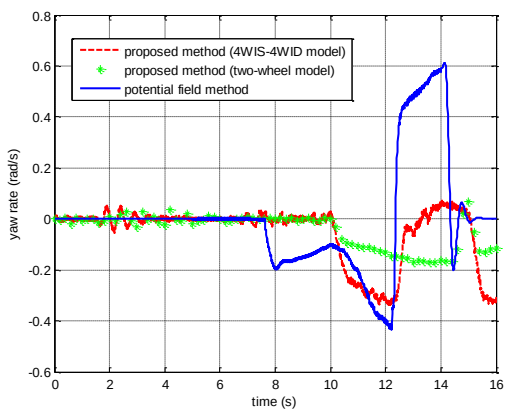

(c)

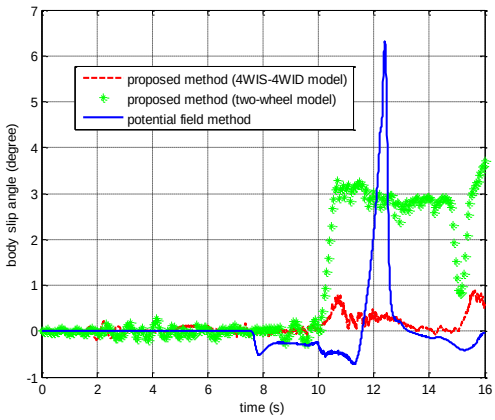

(d)

Figure 4. *The vehicle states in the first set of simulations* ***(a)*** *longitudinal velocity in the global coordinate system* ***(b)*** *lateral velocity in the global coordinate system* ***(c)*** *yaw rate* ***(d)*** *body slip angle*.

Figure 4(c) and Figure 4(d) present the vehicle yaw rate response and body side-slip angle response. In Figure 4(c), the proposed method when applied on the 4WIS-4WID vehicle and two-wheel vehicle has smoother yaw rate response and body side-slip angle when compared with the potential field method, which shows the advantage of the proposed method. In addition, the yaw rate response of the 4WIS-4WID vehicle is larger than two-wheel model. This is because that the 4WIS-4WID vehicle requires more control effects and can change the heading angle more quickly (larger yaw rate) to have better lateral trajectory tracking performance (as shown in Figure 3(b)) and better side-slip angle performance (as shown in Figure 4(d)) compared with two-wheel vehicle. This also proves the 4WIS-4WID vehicle has the advantages of better mobility by changing the heading angle more quickly.

In the second set of simulations, the autonomous vehicle is trying to avoid and overtake the slow vehicle 100 meters ahead. The initial longitudinal velocity of the autonomous vehicle (overtaking vehicle) is 20 m/s and the overtaken vehicle is moving in front of the overtaking vehicle with the longitudinal velocity of 15 m/s. In order to complete the motion of overtaking, the overtaking vehicle is assumed to first decelerate from 20 m/s to 15 m/s in the first 100 meters, and then have a lane change manoeuvre to the right track. After that, the overtaking vehicle speeds up from 15 m/s to 20 m/s in order to go ahead of the overtaken vehicle. Finally, the overtaking vehicle takes another lane change manoeuvre in order to go back to the left track. The details of this scenario are described in Figure 5(a).

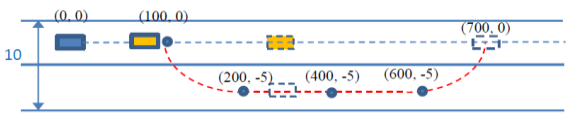

(a)

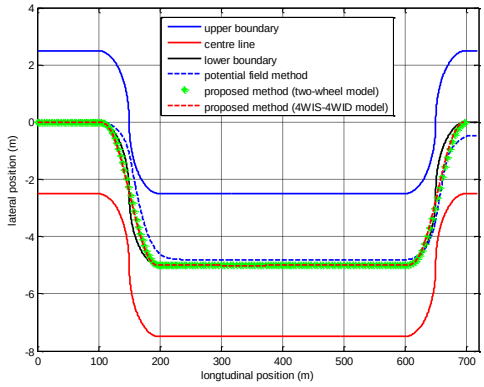

(b)

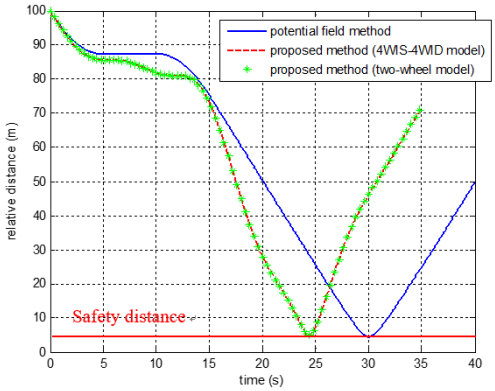

(c)

Figure 5. ***(a)*** *Vehicle overtaking scenario in the second set of simulations (unit: meter).* ***(b)*** *The vehicle trajectory in the global coordinate system.* ***(c)*** *The relative distance between the overtaking vehicle and overtaken vehicle.*

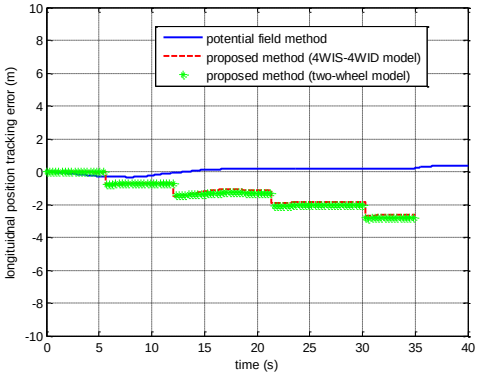

(a)

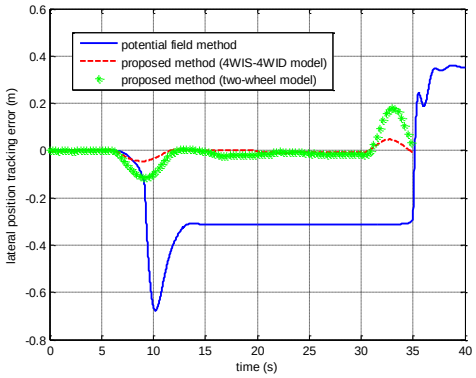

(b)

***Figure 6**. The tracking errors of vehicle trajectory in the second set of simulations **(a)** longitudinal position **(b)** lateral position.*

Figure 5(b) presents the moving trajectory of the controlled overtaking vehicle when both the potential field method and the proposed method (applied on traditional two-wheel vehicle and 4WIS-4WID vehicle) are applied. Both the trajectories of the proposed method when applied on two-wheel vehicle and 4WIS-4WID vehicle are quite smooth and within the road boundary. Figure 5(c) shows that the overtaking vehicle and overtaken vehicle maintain the safety distance to avoid collision. According to Figure 6, the potential field method shows big lateral tracking error compared with the proposed methods based on two-wheel model and four-wheel model, while the longitudinal tracking error of potential filed method is smaller than the proposed methods. It is noted that the lateral tracking error is more important than longitudinal tracking error on highway overtaking scenario, so the proposed method has better overall tracking performance than potential field method. The tracking error of proposed method based on two-wheel model is larger than four-wheel model, especially for the tracking error of the lateral position. This shows the advantages of 4WIS-4WID model.

Figures 7(a) and 7(b) show the longitudinal velocity and lateral velocity in the global coordinate system for both the potential field method and the proposed trajectory planning method. The desired longitudinal velocity and lateral velocity at points (100,0), (200,-5), (400,-5), (600, -5), (700,0) are (V_{xd1}, V_{yd1}), (V_{xd2}, V_{yd2}), (V_{xd3}, V_{yd3}) (V_{xd4}, V_{yd4}), (V_{xd5}, V_{yd5}) respectively. The potential field method can only roughly achieve the desired longitudinal velocity and lateral velocity while the proposed method can accurately achieve desired values. This is due to that the proposed trajectory planning method can not only plan the desired target positions but also the desired longitudinal and lateral velocities at target positions. Figure 7(c) and Figure 7(d) present the vehicle yaw rate and body slip angle performance, which proves that the proposed trajectory planning method can achieve much better handling and stability performance compared with potential field method.

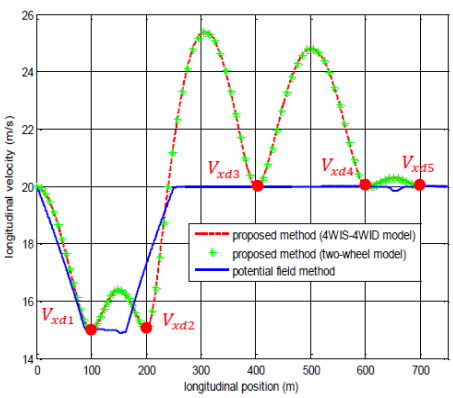

(a)

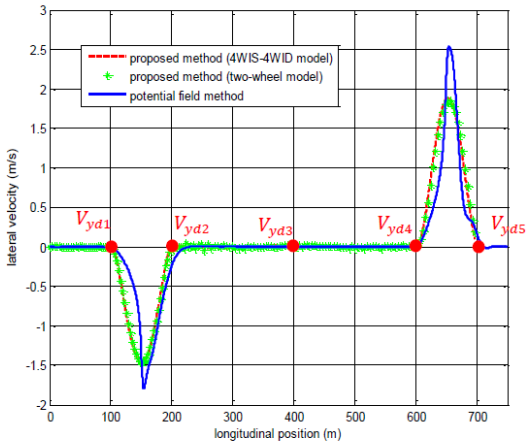

(b)

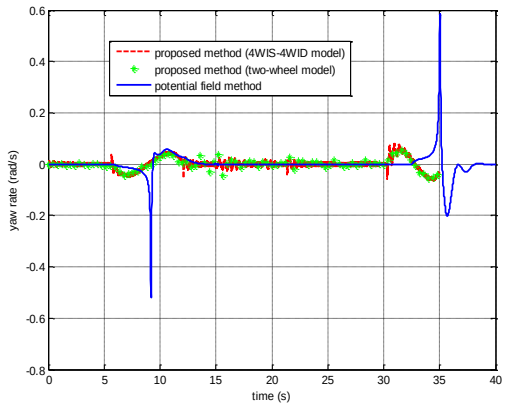

(c)

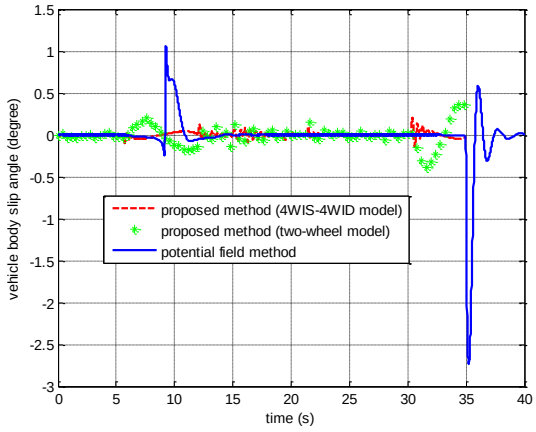

(d)

Figure 7. *The vehicle state in the second set of simulations **(a)** longitudinal velocity in the global coordinate system **(b)** lateral velocity in the global coordinate system **(c)** yaw rate **(d)** body slip angle.*

In the third set of simulations, similar to the second set of simulations, the autonomous vehicle is trying to overtake another vehicle ahead, but the scenario is more challenging. The overtaking vehicle is assumed to move on the highway with three lanes. At the beginning, the overtaking vehicle is moving on the left lane and the initial longitudinal velocity is 20 m/s. One slow vehicle is moving in front of the overtaking vehicle with the longitudinal velocity of 15 m/s. In order to complete the motion of

overtaking, the overtaking vehicle is assumed to first decelerate from 20 m/s to 15 m/s in the first 100 meters, and then have a lane change manoeuvre to the middle lane. However, on the middle lane, there is another slow vehicle (longitudinal velocity is 15 m/s) is moving in front of the overtaking vehicle. The overtaking vehicle has to take another lane change to the right lane. After that, the overtaking vehicle speeds up from 15 m/s to 20 m/s in order to go ahead of the two overtaken vehicles. Finally, the overtaking vehicle takes another two lane change manoeuvres in order to go back to the left track. The details of this scenario are described in Figure 8(a).

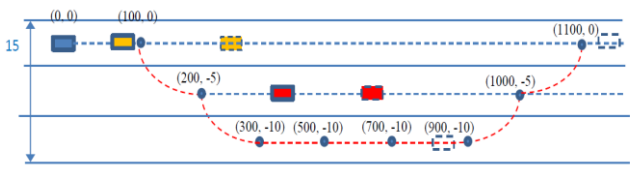

(a)

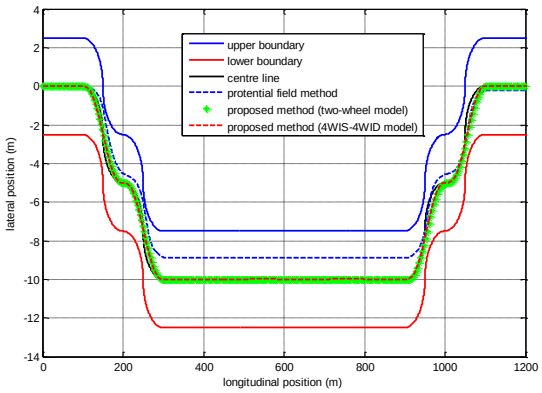

(b)

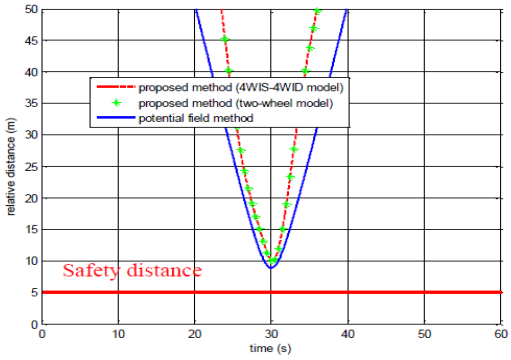

(c)

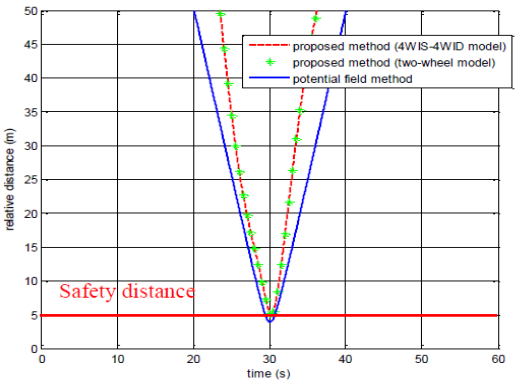

(d)

***Figure 8**. **(a)** The vehicle overtaking scenario in the third set of simulations(unit: meter) **(b)** vehicle trajectory in the global coordinate system in the third set of simulations **(c)**The relative distance between the overtaking vehicle and overtaken vehicle on the left lane **(d)** the relative distance between the overtaking vehicle and overtaken vehicle on the middle lane.*

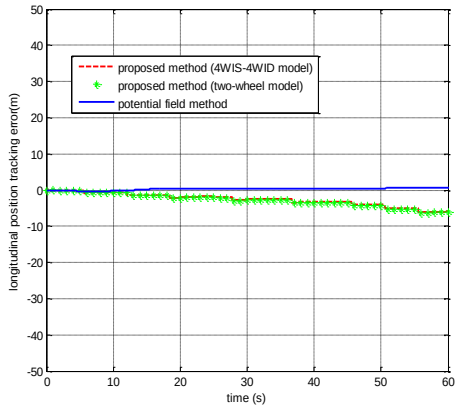

(a)

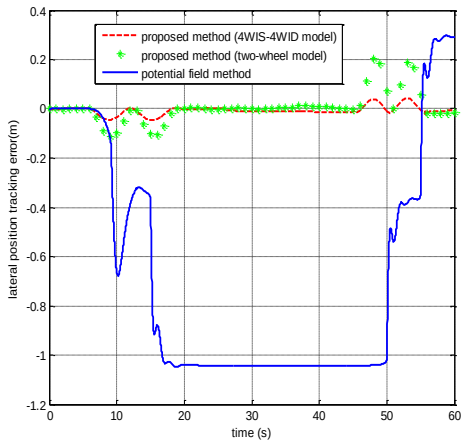

(b)

***Figure 9**. The tracking errors of vehicle trajectory in the third set of simulations **(a)** longitudinal position **(b)** lateral position.*

Figure 8(b) shows that the trajectories of proposed method and potential field method are all constrained within the road boundary. Figure 8(c) shows that the overtaking vehicle and the overtaken vehicle on the left lane maintain the safety distance for all the proposed method and potential field method. Figure 8(d) suggests that, for the potential field method, relative distance between the overtaking vehicle and the overtaken vehicle in the middle lane is smaller than the safety distance. This is quite dangerous and may cause the collision on the highway. The main reason behind this is the big lateral tracking error of the potential field method, which is shown in Figure 9(b). This proves that the proposed method can achieve the better tracking control performance, especially the critical lateral tracking performance on the highway scenario.

Figures 10(a) and 10(b) show the longitudinal velocity and lateral velocity in the global coordinate system for both the potential field method and the proposed

trajectory planning method. The desired longitudinal velocity and lateral velocity at points (100,0), (200,-5), (300,-10), (500,-10), (700, -10), (900, -10), (1000,-5), (1100,0) are (V_{xd1}, V_{yd1}), (V_{xd2}, V_{yd2}), (V_{xd3}, V_{yd3}), (V_{xd4}, V_{yd4}), (V_{xd5}, V_{yd5}),(V_{xd6}, V_{yd6}),(V_{xd7}, V_{yd7}), (V_{xd8}, V_{yd8}), respectively. Similarly, the potential field method can only roughly achieve the desired longitudinal velocity and lateral velocity while the proposed method can accurately achieve desired values. Figures 10(c) and 10(d) show that the proposed method can achieve much better handling and stability control performance compared with the potential field method.

It is noted that in the second and third sets of simulations, the 4WIS-4WID vehicle and two-wheel vehicle show similar simulation responses because the vehicle is moving on the highway scenario with relative stable driving condition and smaller side-slip angle response compared with the intersection turning scenario in the first set of simulations. This is because that the vehicle side-slip angle β is determined by the lateral velocity v_y divided by the longitudinal velocity v_x ($\beta = \tan^{-1}\frac{v_y}{v_x}$). When the values of lateral velocity are similar, the larger longitudinal velocity in the highway scenario ($v_x = 20$m/s) will lead to smaller side-slip angle response compared with the intersection turning scenario ($v_x = 2\sim3$m/s). It can be seen from Figures 4(b), 7(b) and 10(b) that the vehicle lateral velocity for all the three sets of simulations are in the similar range.

On the other hand, in the less stable intersection turning scenario, there is a relatively big difference of the simulation response between the 4WIS-4WID vehicle and two-wheel vehicle and the advantage of 4WIS-4WID can be clearly seen.

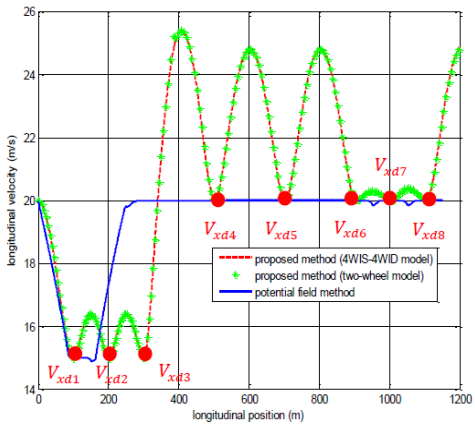

(a)

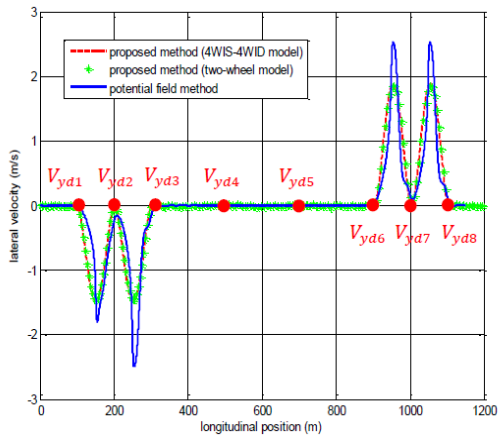

(b)

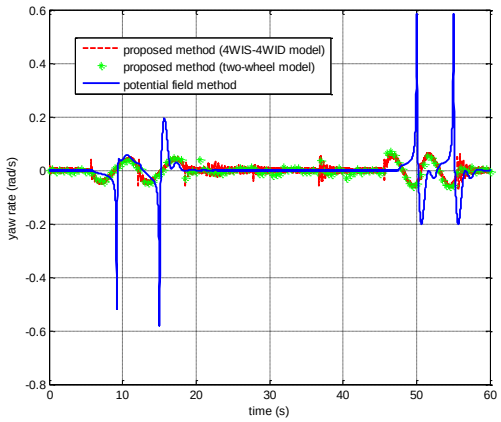

(c)

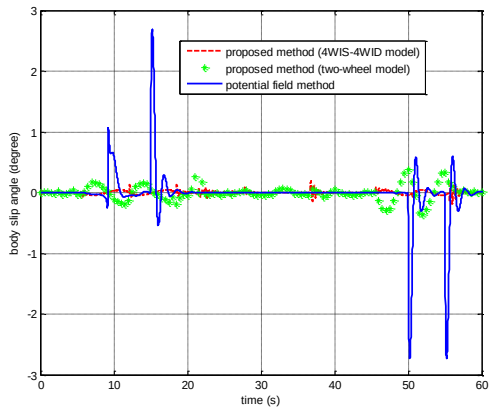

(d)

***Figure 10**. The vehicle state in the third set of simulations **(a)** longitudinal velocity in the global coordinate system **(b)** lateral velocity in the global coordinate system **(c)** yaw rate **(d)** body slip angle.*

6. Conclusion

This study proposes a dynamically integrated spatiotemporal-based trajectory planning and control method for the autonomous vehicles. The upper level trajectory planner can select the best time-parameterised trajectory among a group of the candidate trajectories. After dynamically checking the feasibility of the planned trajectory, the lower level trajectory controller based on the vehicle dynamics model will control the motion of the

vehicle and achieve the desired trajectory. The major findings in the simulation results of this study can be summarised as follows:

1) The proposed trajectory planning and control method can successfully control the motion of autonomous vehicles and achieve the pre-optimised and spatiotemporal-based desired trajectory.

2) The proposed trajectory planner has optimised the spatiotemporal-based trajectory while satisfying the target ending position and velocity, and the simulation results prove that all the target vehicle state values can be achieved by the proposed control method.

3) Compared with the spatial-based method (potential filed method), the proposed spatiotemporal-based method has much better handling and stability performance.

4) Compared with traditional two-wheel vehicle, the 4WIS-4WID electric vehicle can achieve the planned trajectory smaller lateral tracking error.

In the future, to deal with the more complex traffic scenarios or even in the off-road situation, the proposed control method will be tested and further improved.

Appendix

In order to verify the stability of proposed SMC in the trajectory controller, the Lypunove function of sliding surface can be proposed as:

$$V_1 = \frac{1}{2}S_1^2 \tag{A1a}$$

$$V_2 = \frac{1}{2}S_2^2 \tag{A1b}$$

$$V_3 = \frac{1}{2}S_3^2 \tag{A1c}$$

The time derivative of above Lypunov function can be presented as followings:

$$\dot{V}_1 = S_1\dot{S}_1 = S_1\left(\boldsymbol{B_x F} - F_{x,total}\right) = -K_{s1}|S_1| \tag{A2a}$$

$$\dot{V}_2 = S_2\dot{S}_2 = S_2\left(\boldsymbol{B_y F} - F_{y,total}\right) = -K_{s2}|S_2| \tag{A2b}$$

$$\dot{V}_3 = S_3\dot{S}_3 = S_3\left(\left(\boldsymbol{B_r F} - M_{z,total}\right)\right) = -K_{s3}|S_3| \tag{A2c}$$

According to equations (A2a), (A2b) and (A2c), the time derivative of the Lypunov function is always negative, which proves the stability of the SMC.

7. Acknowledgments

This research was supported under Australian Research Council's Discovery Projects funding scheme (project number DP140100303) and the Open Research Fund Program of the State Key Laboratory of Advanced Design and Manufacturing for Vehicle Body, Hunan University (31515001).

8. References

[1] Bureau of Transportation Statistics,: 'National transportation statistics', 2014, U.S.Dept.Transportation.

[2] Bureau of Infrastructure Transport and Regional Economics,: 'Road death Australia', 2014, Canberra ACT, Australia.

[3] He, J., McCarley, J.S., Kramer, A. F.,: 'Lane keeping under cognitive load: Performance changes and mechanisms', *Hum. Factors: J. Hum. Factors Ergon. Soc.*, 2014, 56, pp.414-426.

[4] Werling, M., Kammel, S., Ziegler, J., and Gröll, L.,: 'Optimal trajectories for time-critical street scenarios using discretised terminal manifolds', *The International Journal of Robotics Research*, 2011, 31(3), pp.346-359.

[5] National Highway Traffic Safety Administration,: 'Preliminary statement of policy concerning automated vehicles', 2013, pp.1-14.

[6] Yang, S., Wang, W., Liu, C., Deng, K., Hedrick, J. K.,: 'Feature analysis and selection for training an end-to-end autonomous vehicle controller using the deep learning approach', 2017 IEEE Intelligent Vehicles Symposium (IV), Redondo Beach, 2017, CA, USA, pp.1033-1038.

[7] Ohn-Bar, E., Trivedi, M. M.,: 'Are all objects equal? Deep spatio-temporal importance prediction in driving videos', Pattern Recognition, 2017, 64, pp.425-436.

[8] Sallab, A. E., Abdou, M., Perot, E., Yogamani, S.,: 'Deep reinforcement learning framework for autonomous driving', Electronic Imaging, 2017, 19, pp.70-76.

[9] Wang, F. Y., Zheng, N. N., Cao, D., Martinez, C. M., Li, L., Liu, T.,: 'Parallel driving in CPSS: a unified approach for transport automation and vehicle intelligence', IEEE/CAA Journal Of Automatica SINICA, 2017, 4(4), pp.577-587.

[10] Wang, F. Y.,: 'Parallel control and management for intelligent transportation systems: concepts, architectures, and applications', IEEE Transactions on Intelligent Transportation Systems, 2010, 11(3), pp.630-638.

[11] Li, X., Sun, Z., Cao, D., He, Z., and Zhu, Q.,: 'Real-time trajectory planning for autonomous urban driving: framework, algorithms, and verifications', IEEE/ASME Transactions on Mechatronics, 2016, 21(2), pp.740-753.

[12] Werling, M., Gindele, T., Jagszent, D., Gröll, L.,: 'A robust algorithm for handling moving traffic in urban scenarios', in *IEEE Intelligent Vehicles Symposium*, Eindhoven, 2008, The Netherlands, pp.1108-1112.

[13] Lapierre, L., Zapata, R., Lepinay, P.,: 'Combined path-following and obstacle avoidance control of a wheeled robot', *The International Journal of Robotics Research*, 2007, 26(4), pp.361-375.

[14] Soetanto, D., Lapierre, L., Pascoal, A.,: 'Adaptive, nonsingular path following control of dynamic wheeled robot', *42nd IEEE Conference on Decision and Control*, 2003, Maui, Hawaii, USA, pp.1765-1770.

[15] Ge, S.S., Cui, Y.J.,: 'Dynamic motion planning for mobile robots using potential field method', *Autonomous Robots*, 2002, 13, pp.207-222.

[16] Fletcher, L., Teller, S., Olson, E., Moore, D., Kuwata, Y., How, J., et al.,: 'The MIT-Cornell collision and why it happened', *Journal of Field Robotics*, 2008, 25(10), pp.775-807.

[17] Kuwata, Y, Fiore, G.A., Teo, J., Frazzoli, E., How, J.P.,: 'Motion planning for urban driving using RRT', In *International Conference on Intelligent Robots and Systems*, 2008, Nice, France, pp.1681–1686.

[18] Likhachev, M., Ferguson, D.,: 'Planning long dynamically feasible maneuvers for autonomous vehicles'. *The International Journal of Robotics Research*, 2009, 28(8), pp.933–945.

[19] Pivtoraiko, M., Kelly, A.,: 'Efficient constrained path planning via search in state lattices', *International Symposium on Artificial Intelligence, Robotics, and Automation in Space*, 2005, pp.1-7.

[20] LaValle, M.,: 'Rapidly-exploring random trees: A new tool for path planning', Technical Report, Computer Science Department, 1998, Iowa State University.

[21] Howard, T., Kelly, A.,: 'Optimal rough terrain trajectory generation for wheeled mobile robots',: *The International Journal of Robotics Research*, 2007, 26(2), pp.141–166.

[22] Montemerlo, M., Becker, J., Bhat, S., Dahlkamp, H., Dolgov, D., Ettinger, S., et al.,: 'Junior: The Stanford entry in the Urban Challenge', 2008, *Journal of Field Robotics*, 25(9), pp.569–597.

[23] Elbanhawi, M., Simic, M., Jazar, R.,: 'In the passenger seat: investigating ride comfort measures in autonomous cars', *IEEE Intelligent Transportation System Magazine*, 2015, 7(3), pp.4-17.

[24] Werling, M., Ziegler, J., Kammel, S., Thrun, S.,: "Optimal trajectory generation for dynamic street scenarios in a Frenét Frame", *2010 IEEE International Conference on Robotics and Automation*, 2010, Anchorage Convention District, USA, pp.987-993.

[25] Li, X., Sun, Z., Cao, D., Liu, D. He, H.,: 'Development of a new integrated local trajectory planning and tracking control framework for autonomous ground vehicles', *Mechanical Systems and Signal Processing*, 2017, 87, pp.118-137.

[26] Katrakazas, C., Quddus, M., Chen, W-H, Deka, L.,: 'Real-time motion planning methods for autonomous on-road driving: State-of-the-art and future research directions', *Transportation Research Part C*, 2015, 60, pp.416-442.

[27] Dugoff, H., Fancher, P.S., Segel, L.,: 'An analysis of tire traction properties and their influence on vehicle dynamic performance', *SAE 700377*, 1970, pp.1219-1243.

[28] Levinson, J., Montemerlo, M., Thrun, S.,: 'Map-based precision vehicle localization in urban environments', in *Robotics: Science and Systems*, 2007, 4, Cambridge, MA, USA: MIT Press, 2007, p.1.

[29] Levinson, J and Thrun, S.,: 'Robust vehicle localization in urban environments using probabilistic maps', in *Proc. IEEE Int. Conf. Robot. Autom.*, 2010, Anchorage, AK, USA, pp. 4372–4378.

[30] Park, H., Gerdes, J.C.,: 'Optimal tyre force allocation for trajectory tracking with an over-actuated vehicle', *2015 IEEE Intelligent Vehicles Symposium (IV)*, 2015, Seoul, Korea, pp.1032-1037.

[31] Boada, B., Boada, M., Díaz, V.,: 'Fuzzy-logic applied to yaw moment control for vehicle stability,' *Vehicle System Dynamics*, 2005, 43, pp.753-770.